

Electronic Supplementary Information

### Mixed-anion mixed-cation perovskite (FAPbI<sub>3</sub>)<sub>0.875</sub>(MAPbBr<sub>3</sub>)<sub>0.125</sub>: an ab initio molecular dynamics study

Eduardo Menéndez-Proupin<sup>1,2</sup>, Shivani Grover<sup>3</sup>, Ana L. Montero-Alejo<sup>4</sup>, Scott D. Midgley<sup>3</sup>, Keith T. Butler<sup>5</sup> and Ricardo Grau-Crespo<sup>3,\*</sup>

<sup>1</sup> Departamento de Física Aplicada I, Escuela Politécnica Superior, Universidad de Sevilla, Seville E-41011, Spain

<sup>2</sup> Departamento de Física, Facultad de Ciencias, Universidad de Chile, Casilla 653, Santiago, Chile

<sup>3</sup> Department of Chemistry, University of Reading, Whiteknights, Reading RG6 6AD, UK

<sup>4</sup> Departamento de Física, Facultad de Ciencias Naturales, Matemática y del Medio Ambiente (FCNMM), Universidad Tecnológica Metropolitana, José Pedro Alessandri 1242, Ñuñoa, Santiago 7800002, Chile

<sup>5</sup> SciML, Scientific Computing Division, Rutherford Appleton Laboratory, Harwell, UK

\* Corresponding author. Email: [r.grau-crespo@reading.ac.uk](mailto:r.grau-crespo@reading.ac.uk)

#### Probabilities in SQS model

In a random solution (FAPbI<sub>3</sub>)<sub>1-x</sub>(MAPbBr<sub>3</sub>)<sub>x</sub> the probability of finding  $n$  Br ions as nearest neighbors to the MA (out of  $N=12$  halides) is given by the binomial distribution  $P(n) = C(N, n)x^n(1-x)^{N-n}$ . The values for  $x = 0.125$  are listed in Table S1 in the column "Ideal  $P(n)$ ". The column "Model  $P(n)$ " list the best approximating fractions  $m/8$ , which are the fractions that can be realized in 2x2x2 supercells containing eight cation sites.

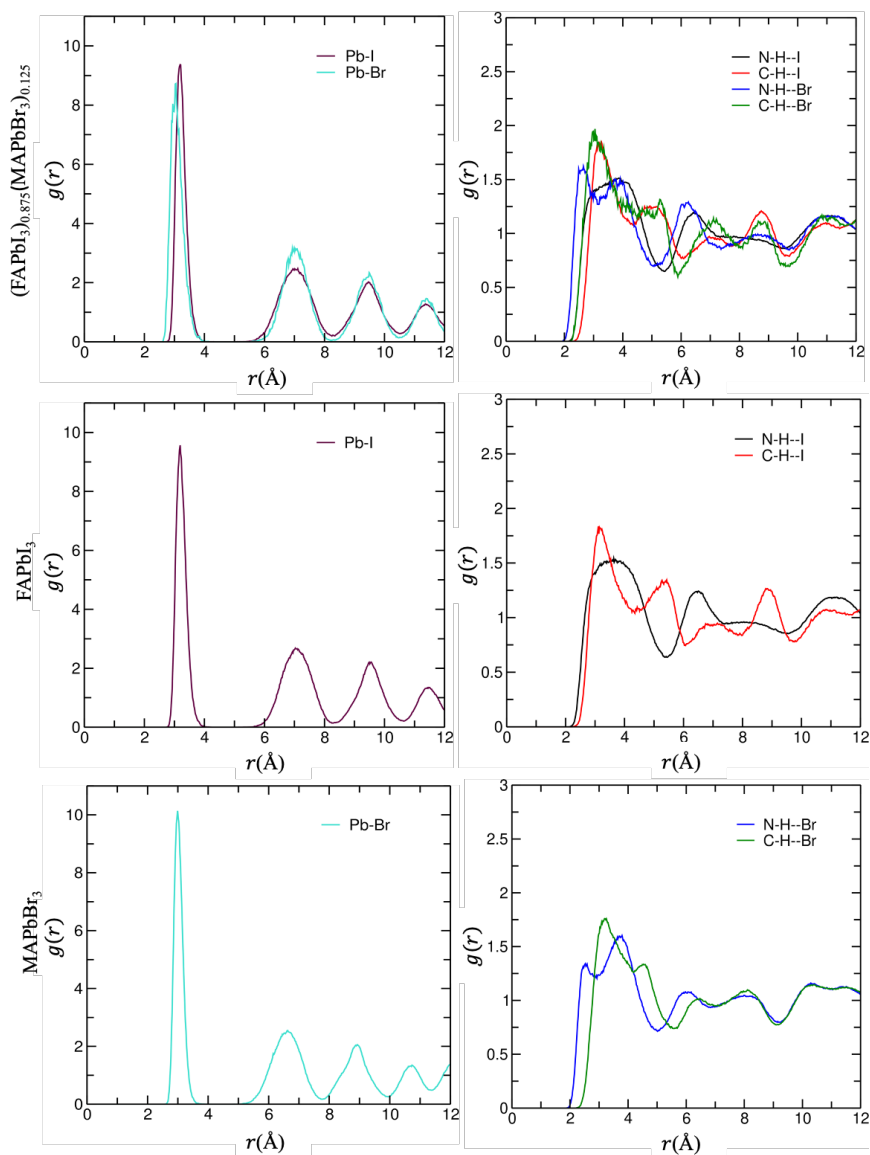
**Table S1.** Probability of finding  $n$  Br ions as nearest neighbors to the MA (out of  $N=12$  halides in the first coordination sphere around MA). The ideal probability, as given by the binomial distribution  $P(n) = C(N, n)x^n(1-x)^{N-n}$ , corresponds to random occupation. The model probabilities are limited to fractions of 8, as the 2x2x2 supercell contains 8 MA cations.

$n$	Ideal $P(n)$	Model $P(n)$
0	0.201	2/8=0.250
1	0.345	3/8=0.375
2	0.271	2/8=0.250
3	0.129	1/8=0.125
4	0.042	0
5	0.009	0
6	0.002	0
7	0.0002	0
8	0.0001	0
9	0.0000	0
10	0.0000	0
11	0.0000	0
12	0.0000	0

## Structural properties

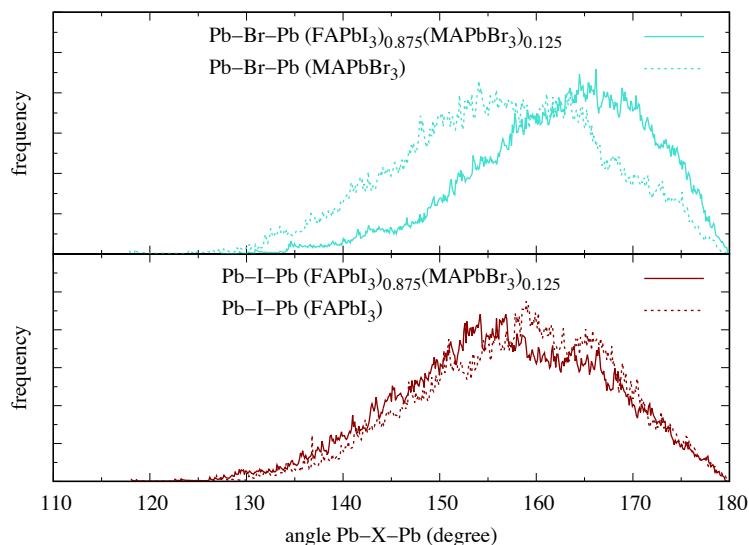
Here, some data derived from the analysis of the MD simulations are presented. Figure S1 contains the same data of Figure 1 of the main text, but the curves organized in separate plots for each compound.

Figure S2 shows the same data of Figure 2, but Pb-Br-Pb and Pb-I-Pb angle distributions are shown in separated plots.

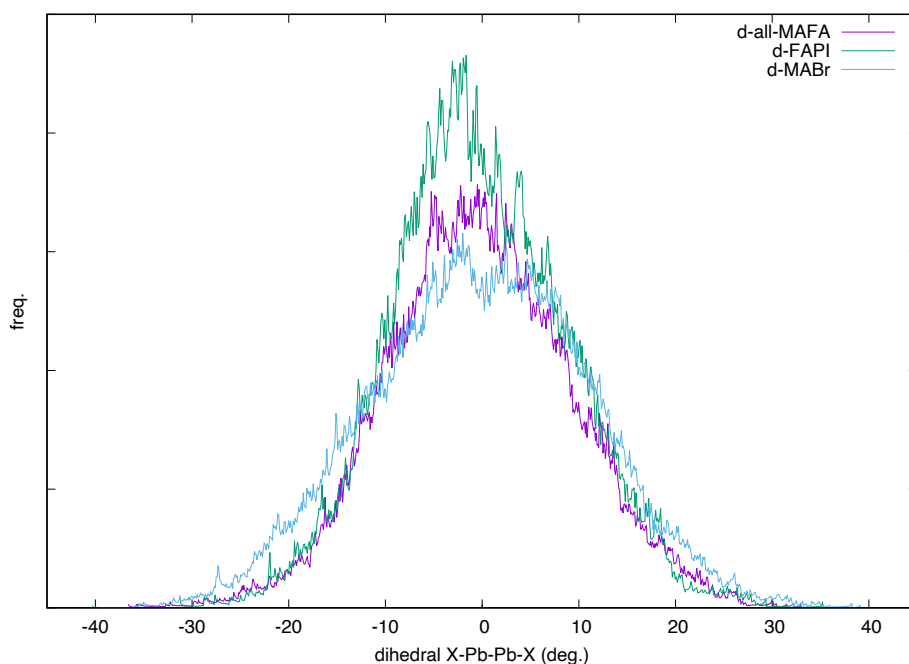


**Figure S1.** Partial pair distribution functions for species Pb-I and Pb-Br (left panel) and H-halide (right panel), differentiating the cases where H is bound to N or C.

Figure S3 shows the distribution of dihedral angles X-Pb-X-Pb for all compounds. As discussed in the main text, the absence of bimodal distributions signals the absence of octahedra rotations characteristic of the perovskite tetragonal phase.

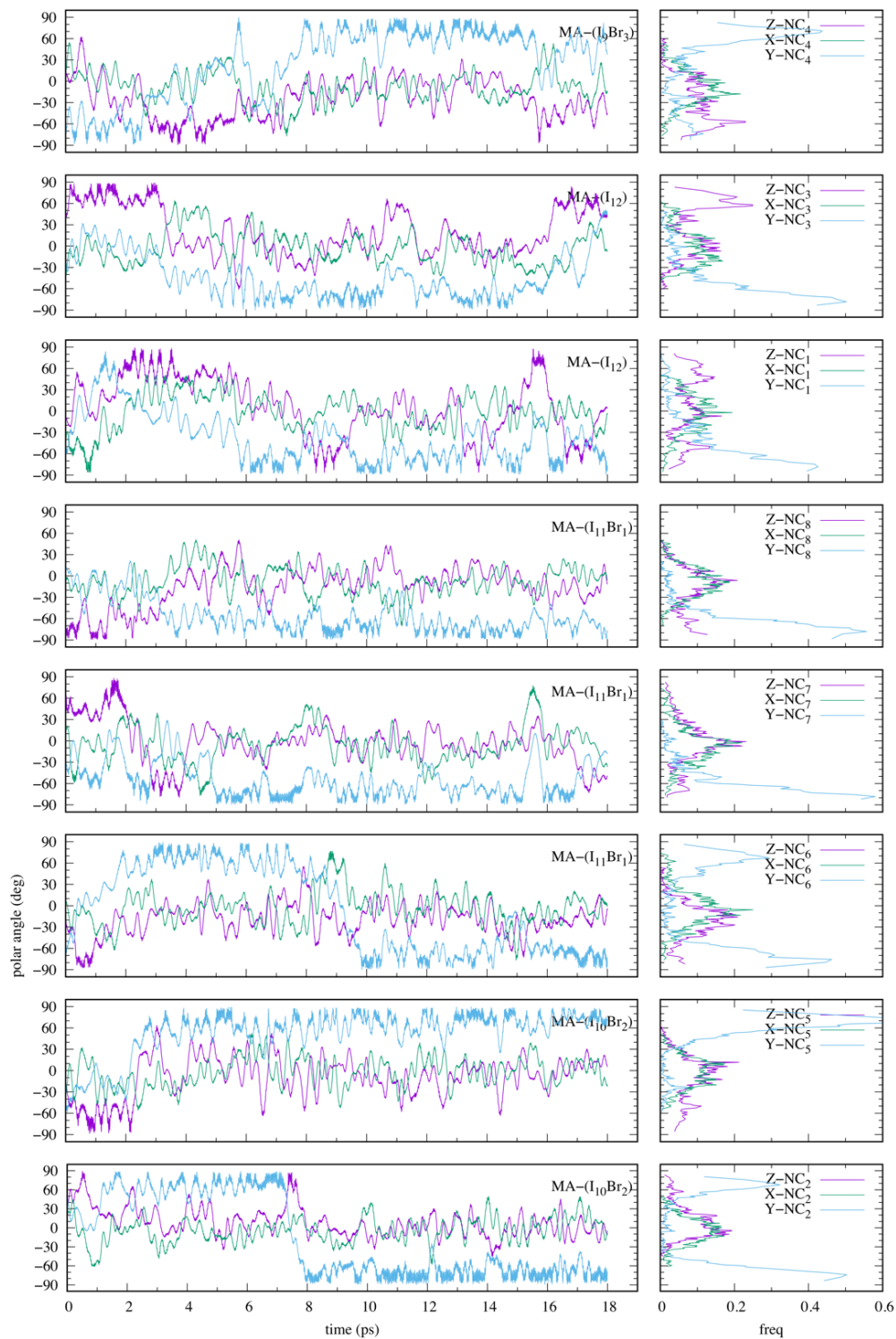


**Figure S2.** Distribution of angles Pb-X-Pb (X=Br, or I) in the three compounds. Solid lines correspond to  $(\text{FAPbI}_3)_{0.875}(\text{MAPbBr}_3)_{0.125}$ , while dashed lines correspond to  $\text{FAPbI}_3$  and  $\text{MAPbBr}_3$ .

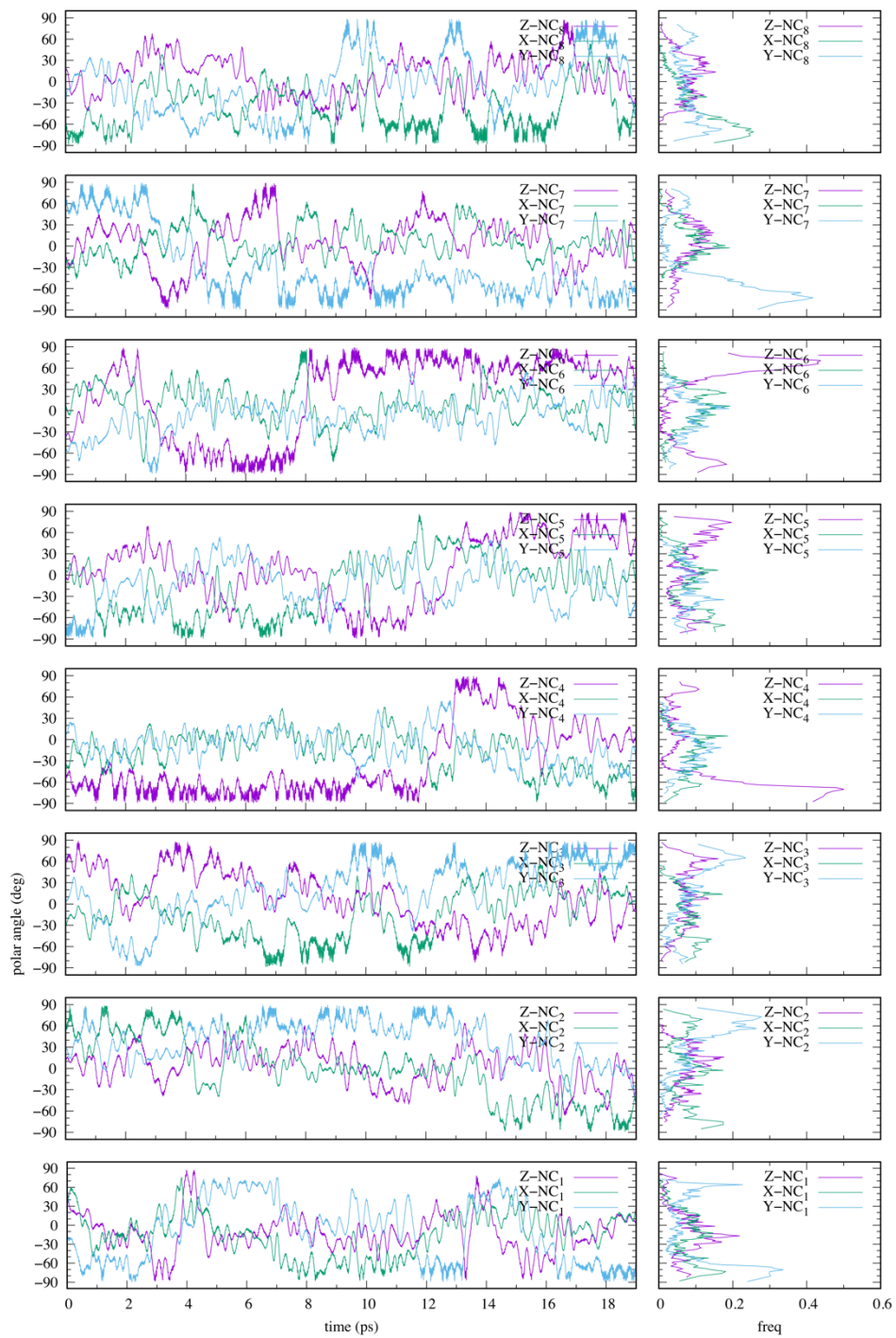


**Figure S3.** Distribution of dihedral angles X-Pb-Pb-X (including the measurement along each cell vector) in  $(\text{FAPbI}_3)_{0.875}(\text{MAPbBr}_3)_{0.125}$ .

Figure S4 shows the time evolution of the angle formed by the vector C-N in the  $\text{MA}^+$  with each cartesian axis for all  $\text{MA}^+$  in  $(\text{FAPbI}_3)_{0.875}(\text{MAPbBr}_3)_{0.125}$ . Figure S5 shows the same evolution for eight  $\text{MA}^+$  in  $\text{MAPbBr}_3$ .



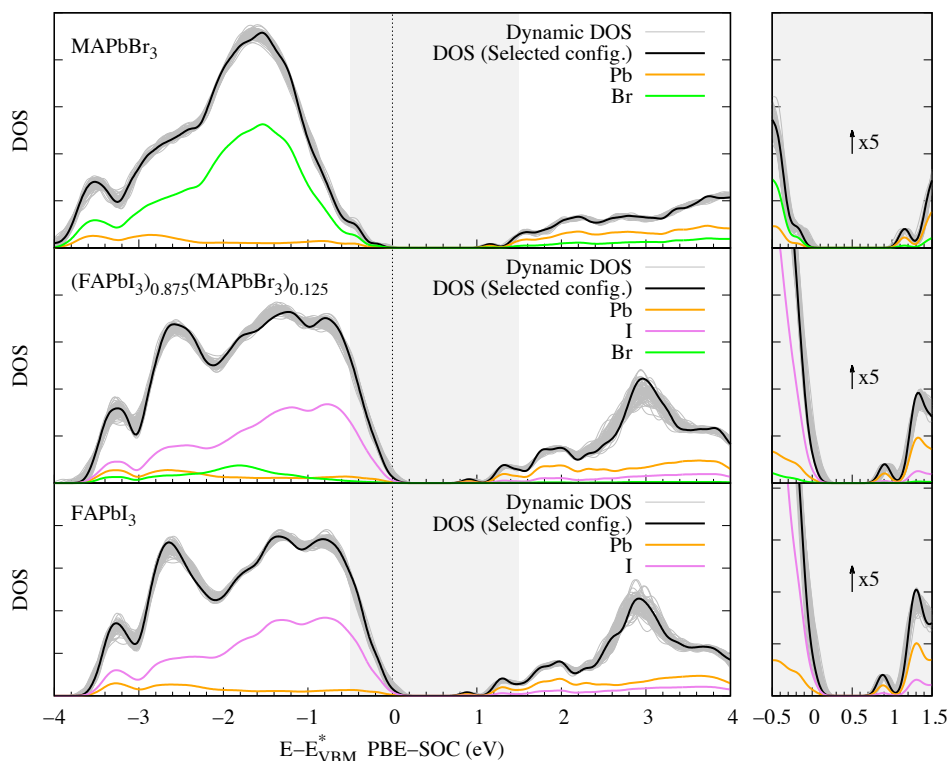
**Figure S4.** Time evolution of the polar angle of vector C-N (MA<sup>+</sup>) with respect to each cartesian axis in (FAPbI<sub>3</sub>)<sub>0.875</sub>(MAPbBr<sub>3</sub>)<sub>0.125</sub>. These cations are surrounded by 0 to 3 Br atoms.



**Figure S5.** Time evolution of the polar angle of vector C-N (MA<sup>+</sup>) with respect to each cartesian axis in MAPbBr<sub>3</sub>. These cations are surrounded by 12 Br atoms.

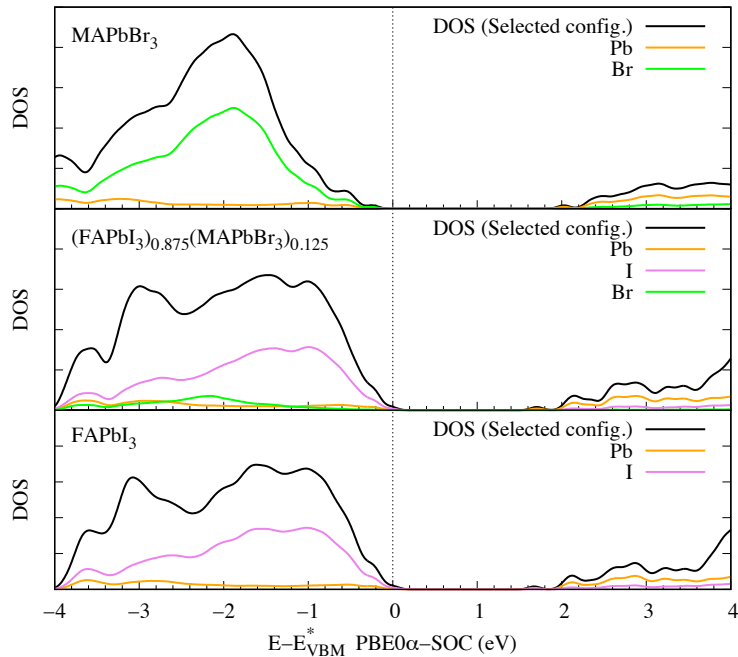
## Electronic structure

Figure S6 shows the total and projected density of states (DOS) of the three studied compounds, as given by DFT calculations with the PBE exchange-correlation functional. The calculations include the spin-orbit coupling (SOC). The total DOS is shown for a set of 70 configurations taken from the MD ensemble. The projected DOS have been obtained for a selected configuration that have DOS close the average DOS of the ensemble. For this configuration, the total and projected DOS have been computed with the PBE0( $\alpha=0.188$ ) functional, and shown in Figure S7 and 7. In fact, Figure S7 is a rescaled version of Figure 7.



**Figure S6.** Average DOS of the solid solution and the pure compounds computed at PBE-SOC level. The gray lines (Dynamic DOS) comprise the DOS of 70 configurations of the MD ensembles. The other lines show the DOS and PDOS of a selected configuration from the MD that matches the band edges of the average. All energies are referred to the VBM of FAPbI<sub>3</sub>. The energy scales of (FAPbI<sub>3</sub>)<sub>0.875</sub>(MAPbBr<sub>3</sub>)<sub>0.125</sub> and MAPbBr<sub>3</sub> are shifted to align the average Pb core level energies with that in FAPbI<sub>3</sub>.

Figure S8 shows the computed imaginary part of the dielectric function computed with the PBE0( $\alpha=0.188$ ) (solid lines) and HSE06 functionals. As discussed in the main text, this calculation has been made using only the gamma point. The large number of atoms and the high cost of hybrid functional calculations have not allowed using a k-point grid. Hence, this function is just a rough approximation and cannot be compared with experimental dielectric functions. For example, it shows a peak at the bandgap, where a van-Hove singularity is expected. However, it allows to establish the coincidence between the bandgap and the optical gap, neglecting exciton effects.



**Figure S7.** DOS and PDOS of the solid solution and the pure compounds computed at hybrid PBE0( $\alpha = 0.188$ )-SOC.  $E_{VBM}^*$  is the VBM state energy of the FAPbI<sub>3</sub> selected configuration. The energy scales of (FAPbI<sub>3</sub>)<sub>0.875</sub>(MAPbBr<sub>3</sub>)<sub>0.125</sub> and MAPbBr<sub>3</sub> are shifted to align the average Pb core level energies with that in FAPbI<sub>3</sub>.

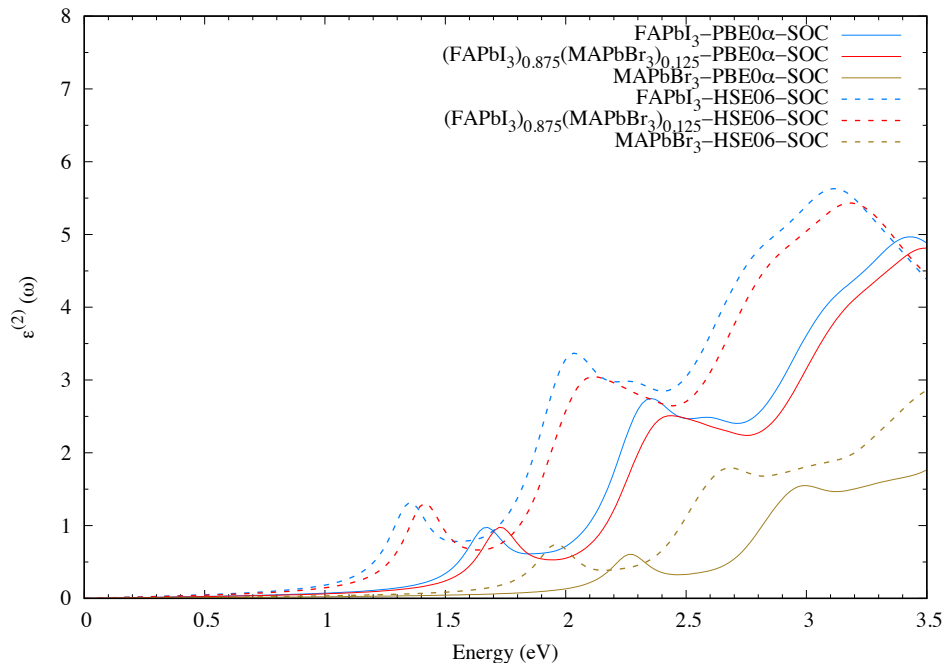


**Figure S8.** Imaginary part of the dielectric function of the solid solution and the pure compounds computed with the functionals PBE0( $\alpha = 0.188$ ) (solid lines) and HSE06 (dashed lines) with SOC.

Figure S9 shows the Tauc's plots applied to experimental absorption spectra, which allow to obtain the optical gaps (equivalent to the bandgaps, as discussed above) reported in Table 2 of the main

text.

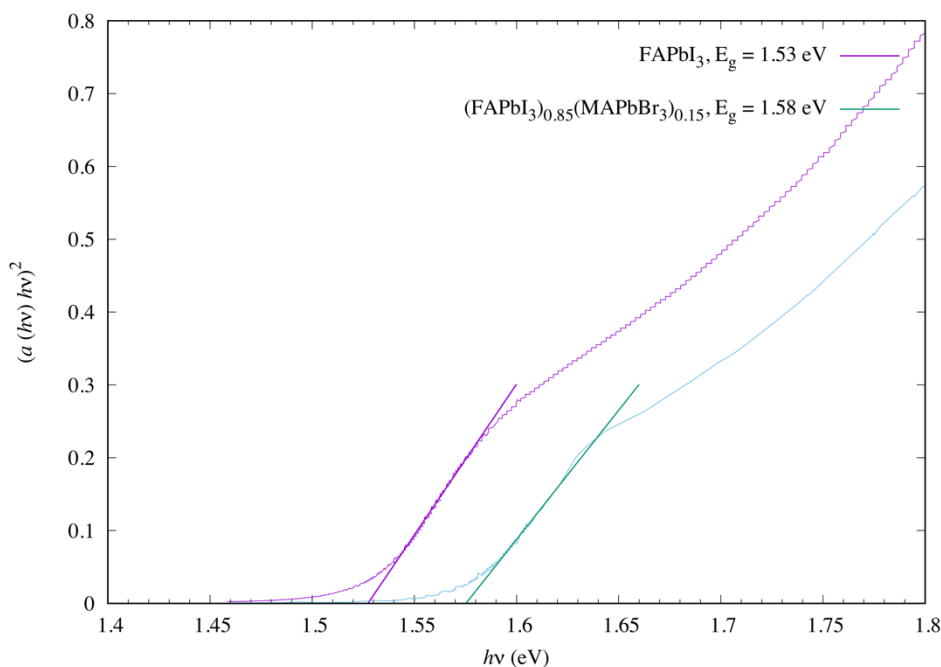


**Figure S9.** Tauc's plot with the absorbance data reported in Ref. Jeon et al (Nature, 2015).

### Data of molecular dynamics simulations

The figures S10, S11, and S12 show the total energy and potential energy along the MD run of  $(\text{FAPbI}_3)_{0.875}(\text{MAPbBr}_3)_{0.125}$ ,  $\text{MAPbBr}_3$  and  $\text{FAPbI}_3$ . Hybrid halide perovskites display a configurational landscape defined by i) the orientation of the organic cations, and ii) the distortion of the inorganic  $\text{PbX}_3$  backbone from the ideal perovskite structure, iii) the symmetry of the Bravais lattice, which changes in a series of phase transitions. In this study, the iii) variability has not been studied, keeping the  $4 \times 4 \times 4$  supercells with constant volume and cubic shape, therefore imposing cubic symmetry as is typical of halide perovskites at high temperature. Local distortions of are allowed, as a rather big supercell has been used, but the long-range lattice distortion that is measured by crystallography is not allowed. Landscape variability i) and ii) are allowed in our fixed supercell simulations.

A sufficiently long MD should sample all the configuration space, and the results should be independent on the starting structure selected. It is not obvious to figure out the optimal length of the MD run, and how long is the equilibration time. In order to evaluate the possible bias due to selecting a particular starting configuration or the thermostat, two starting structures have been considered for  $(\text{FAPbI}_3)_{0.875}(\text{MAPbBr}_3)_{0.125}$  and  $\text{MAPbBr}_3$ . For  $(\text{FAPbI}_3)_{0.875}(\text{MAPbBr}_3)_{0.125}$  both structures A and B start with the  $\text{PbX}_3$  backbone at ideal positions. In structure A, the MA and FA cations are randomly oriented, while in structure B, all cations of the same type present the same, but still arbitrary, orientation. Moreover, two thermostats have been tested: i) the popular Nose-Hoover chain (NHC) [Martyna et al (1992)] and ii) canonical sampling through velocity rescaling (CSVR) [Busi et al. (2007)]. With both thermostats, the first 2 ps have been carried with the so-

called massive thermostat, i.e., one thermostat for each atom. This should be useful to accelerate the energy equipartition in the context of atoms with too different masses, i.e., H and Pb.

It can be appreciated that both starting structures and both thermostats lead to the same total energies, as well as similar times to reach a stable energy. With the NHC thermostat the energy display pronounced oscillations during the first 100 fs, the instantaneous temperature reaching a maximum value of 527 K at  $t=24$  fs. This behavior is typical of the NHC thermostat when the initial structure is not of minimal energy, and it could destroy the fragile hybrid halide perovskite structure. However, the energy oscillations keep under control thanks to the massive thermostat with the low time constant (10 fs). With CSV thermostat, the instantaneous temperature never exceeded 380 K. This could be useful to keep the structure undamaged, but in this case there is no difference for the equilibrated state. With the CSV, the potential and total energies descend faster at the beginning, but in the range 1500-2000 fs the NHC energies are lower. After 2000 fs, the time constant has been changed to 100 fs, a value that means a weaker interaction of the thermostat with the interatomic dynamics and is recommended for sampling in the CP2K manual. One can see that the potential energy keeps descending slowly, and the system has been considered equilibrated just after 5 fs. One can see no advantage either in any of both thermostats, or of any of both initial structures, to optimize the equilibration time. The equilibration time was determined not only from the stabilization of the energies, but also from a qualitative analysis of the histograms of energy distribution. After the 5 fs, the histogram of total energy shows an approximate normal distribution. The simulation with the fully disordered starting structure and the NHC thermostat has been carried out until 23 fs.

For  $\text{MAPbBr}_3$  only the NHC thermostat has been used, but there are also two initial structures. Structure A is an optimized structure, with random orientation of the MA cations and distorted inorganic backbone. This structure was adapted from the polymorphic  $\text{MAPbI}_3$  structure of Zhao et al. (2020), replacing the I by Br, changing the lattice parameter and relaxing it. Structure B has the  $\text{PbBr}_3$  backbone at the ideal positions, but the MA cations are randomly oriented, and the structure was not relaxed. One can appreciate in Figure S12 that the energies of both simulations converge, from above and below, to the same values. The system was considered equilibrated after 6 ps. The simulation from structure A was continued up to 26 ps.

For  $\text{FAPbI}_3$ , only the NHC thermostat was used. The initial configuration was taken from a published optimized structure (Dalpian et al., 2019). The massive thermostat was not applied in this case, although a reduced time constant was used until 8 ps. The system was considered equilibrated after this time.

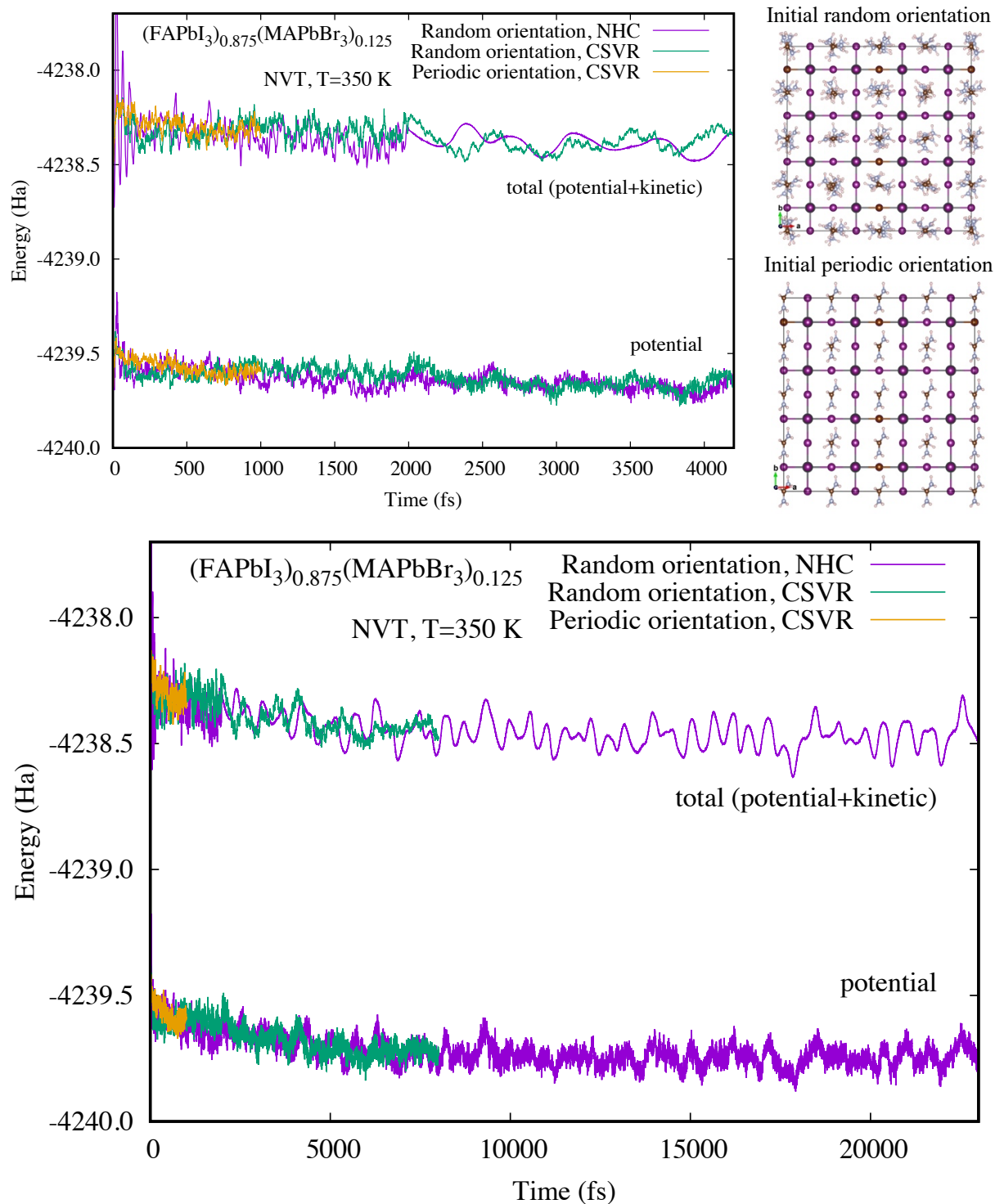


**Figure S10.** Trace of the potential energy (lower lines) and the total energy (upper lines) during the MD simulation of  $(\text{FAPbI}_3)_{0.875}(\text{MAPbBr}_3)_{0.125}$ . The maximum simulation time is 23 ps. NHC and CSVR refer to the thermostat used. Two starting structures are considered: one with fixed orientations of the FA and MA (periodic orientation) and other with every FA and MA of the supercell with random orientation.

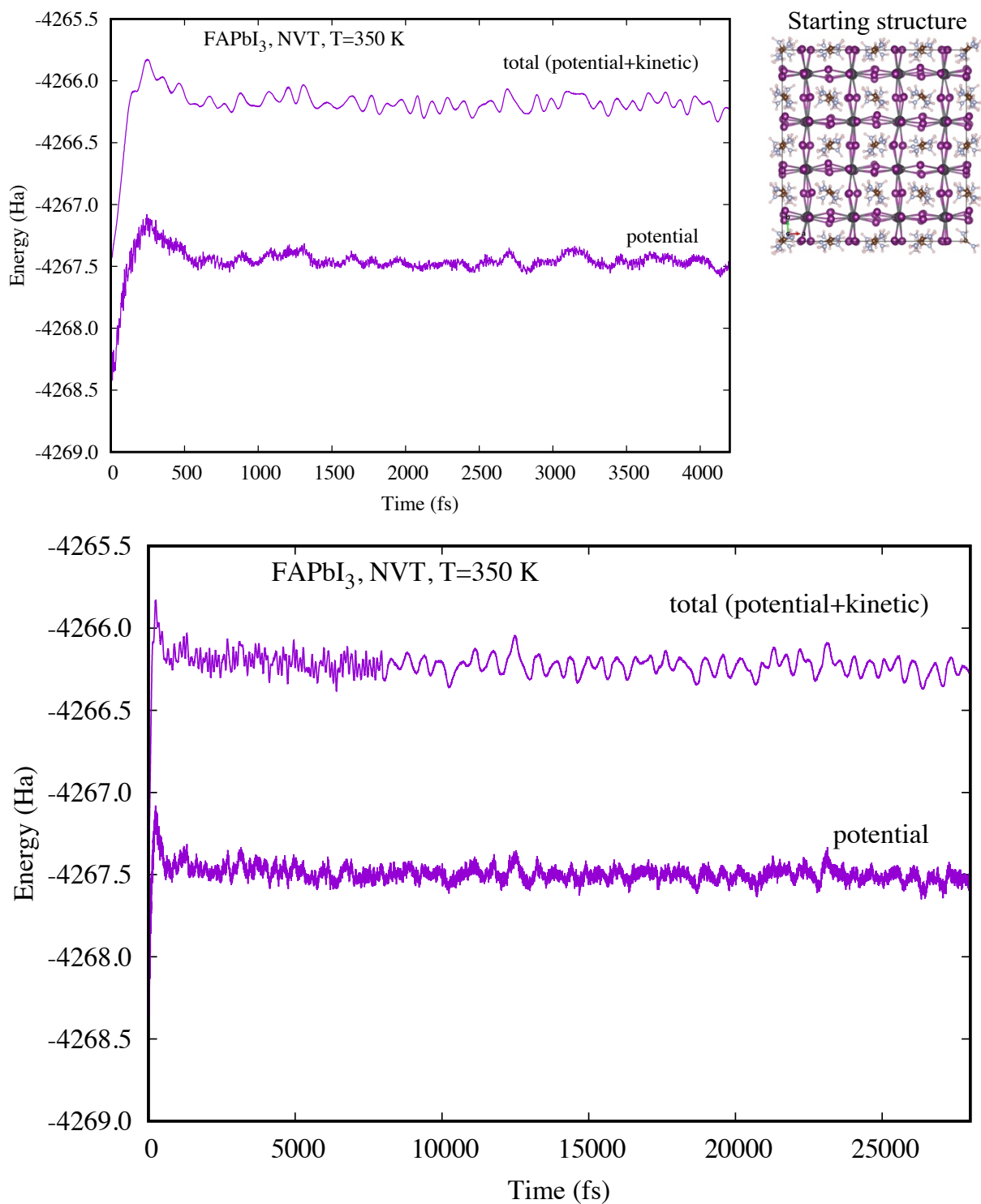


**Figure S11.** Trace of the potential energy (lower lines) and the total energy (upper lines) during the MD simulation of FAPbI<sub>3</sub>. The maximum simulation time is 28 ps. The NHC thermostat was used. The starting structure is from Dalpian et al. (2019)

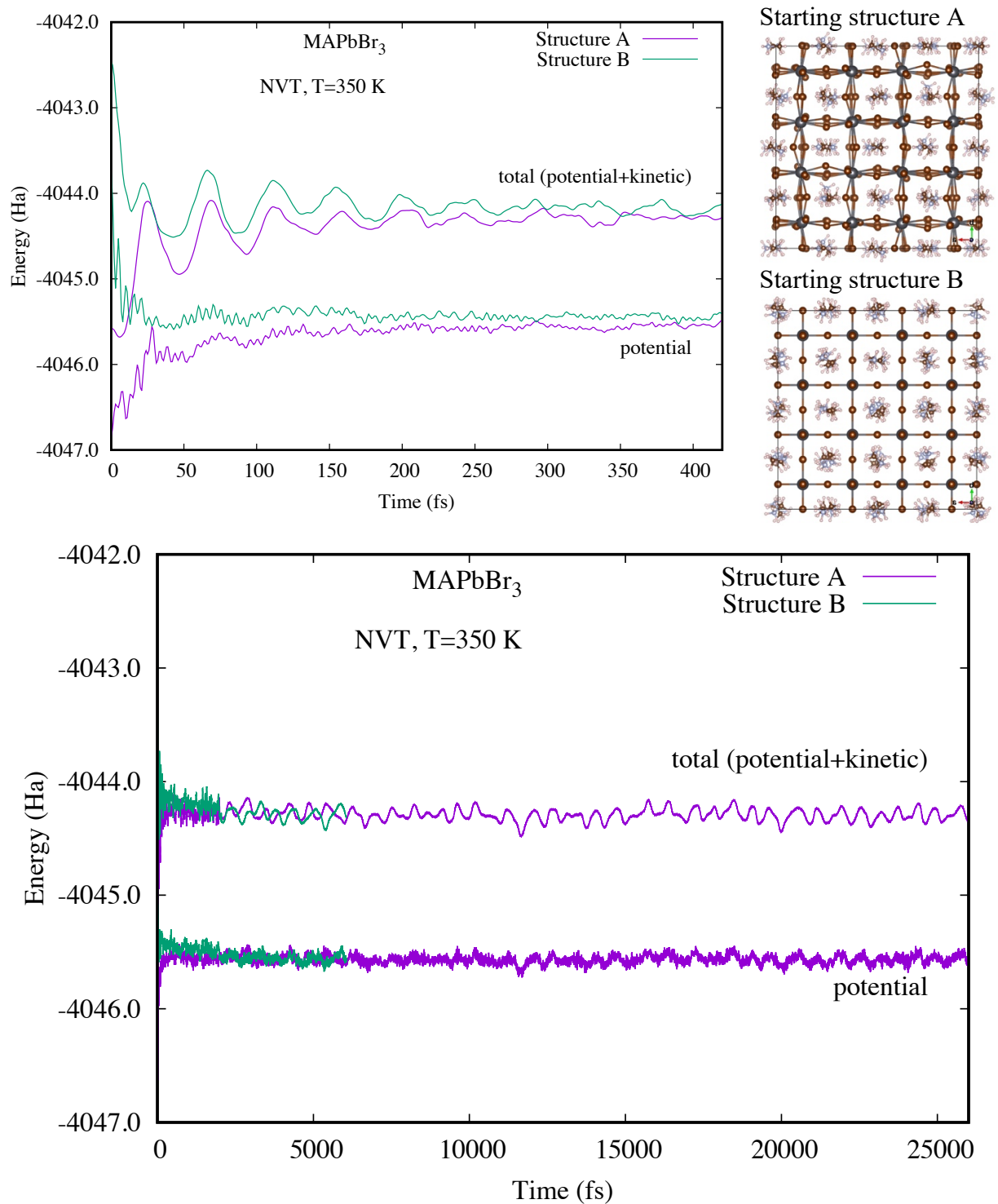


**Figure S12.** Trace of the potential energy (lower lines) and the total energy (upper lines) during the MD simulation of MAPbBr<sub>3</sub>. The maximum simulation time is 26 ps. The NHC thermostat was used. The two starting structures are displayed.

## Correlation between the electronic structure and geometry

Figure S13 shows the correlation between the bandgap with the distributions Pb-X (X=Br, I) bond lengths and Pb-X-Pb angles, which are characterized by average values and standard deviations.

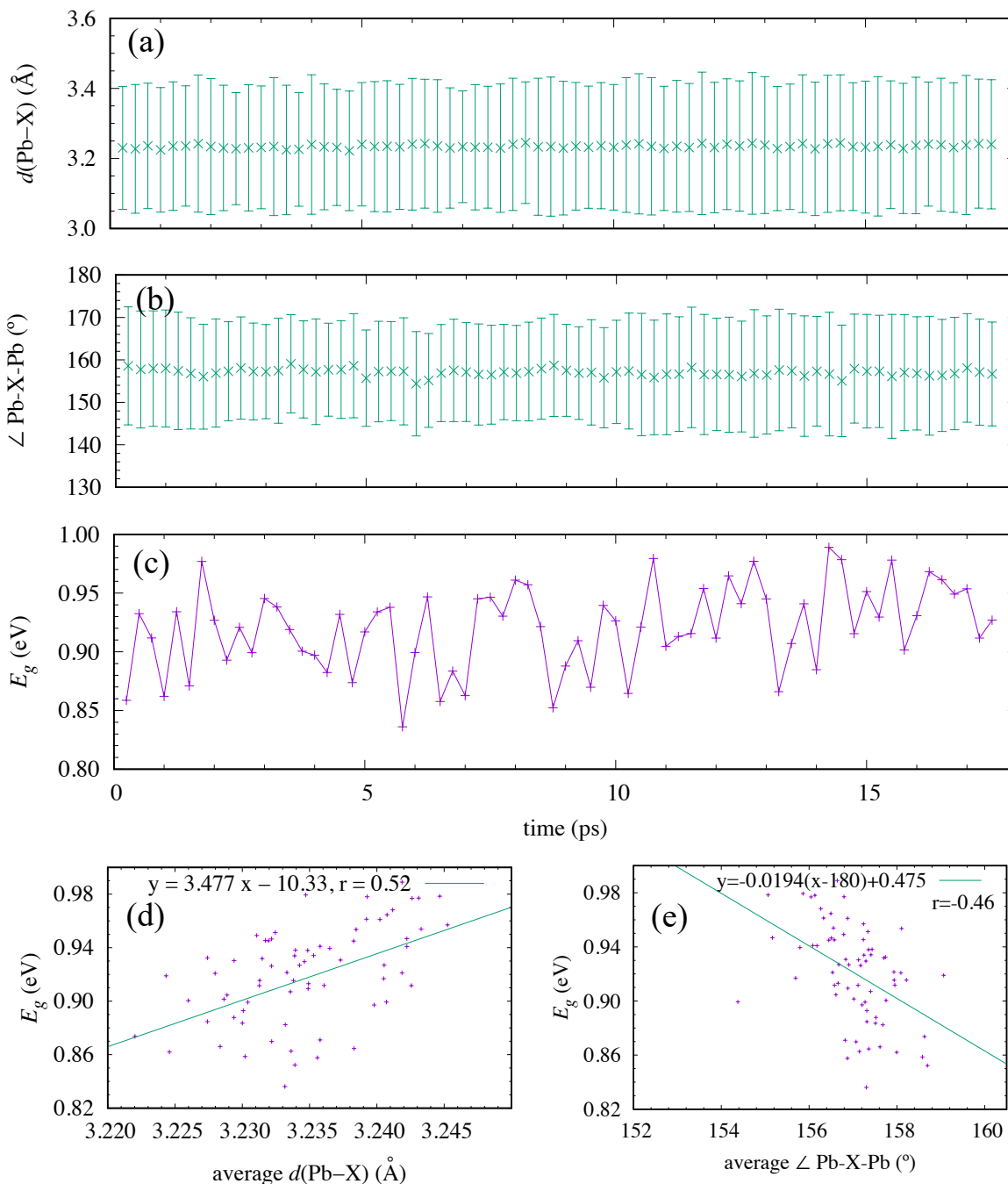


**Figure S13.** Time trace of Pb-X (X=Br,I) average bond length (a), Pb-X-Pb angle (b), and bandgap (c), along 70 configurations of the MD simulation of  $(\text{FAPbI}_3)_{0.875}(\text{MAPbBr}_3)_{0.125}$ . The error bars indicate the standard deviations. The correlation plots between the bandgap (PBE -SOC) and average Pb-X distance (d) and the average Pb-X-Pb angles (e) are also shown. The linear fit equations and correlation coefficients are shown in (d) and (e).

## References

Giovanni Bussi, Davide Donadio, and Michele Parrinello, Canonical sampling through velocity rescaling, *J. Chem. Phys.* **126**, 014101 (2007); <https://doi.org/10.1063/1.2408420>

Glenn J. Martyna, Michael L. Klein, Mark Tuckerman, Nosé–Hoover chains: The canonical ensemble via continuous dynamics, *J. Chem. Phys.* **97**, 2635 (1992); <https://doi.org/10.1063/1.463940>

Gustavo M. Dalpian, Xin-Gang Zhao, Lawrence Kazmerski, and Alex Zunger, Formation and Composition-Dependent Properties of Alloys of Cubic Halide Perovskites. *Chemistry of Materials* **31**, 2497 (2019). <https://doi.org/10.1021/acs.chemmater.8b05329>

Xin-Gang Zhao, Gustavo M. Dalpian, Zhi Wang, and Alex Zunger, Polymorphous nature of cubic halide perovskites, *Phys. Rev. B* **101**, 155137 (2020). <https://doi.org/10.1103/PhysRevB.101.155137>